Laser–driven Positronium excitation in the AEGIS antimatter experiment at CERN

F. Castelli

Dipartimento di Fisica, Università degli Studi di Milano, and INFN Sezione di Milano, Italy

M.G. Giammarchi

Istituto Nazionale di Fisica Nucleare - Sezione di Milano, Italy

Summary. — We present the physics and the antihydrogen production strategy of the AEGIS experiment at CERN. This strategy is based on a series of steps in which Positronium (Ps), produced by e^+ impinging on a porous target, is laser excited to high-n (Rydberg) levels and then made to interact with ultracold antiprotons (around 100 mK). An antihydrogen beam is then formed by Stark acceleration to be sent through a Moirè deflectometer to measure g for antimatter. The efficiency of the antihydrogen production process depends critically on the Positronium excitation process which will be described in detail in the paper. The Ps cloud is produced within a relatively strong magnetic field at 1 T, with a consequent deep modification of Rydberg levels structure. A two–step laser light excitation is proposed, and the physics of the problem is discussed. We derive simple expressions giving the Ps excitation probability with feasible laser pulses suitably tailored in power and spectral bandwidth.

PACS 04.80.Cc – Experimental tests of gravitational theories.
PACS 36.10.Dr – Positronium.
PACS 32.80.Ee – Rydberg states.

1. – Introduction

The experiment AEGIS [1], recently approved at CERN, focuses on studies of fundamental physics with antimatter. During the first phase of the experiment, the production of a antihydrogen ($\overline{H}$) beam is foreseen to allow tests of the Weak Gravitational Principle. The technique relies on the $Ps^* \, \overline{p} \rightarrow \overline{H}^* e^-$ (charge exchange) reaction for producing antihydrogen; a beam is then formed with $\sim$ 500 m/s velocity by means of acceleration in an electric field gradient. The antiatoms are sent on a high sensitivity Moirè classical deflectometer for the measurement of g of antimatter, a quantity that has never been measured before. In a second phase of the experiment, antihydrogen will be slowed down, laser–cooled and confined, to perform higher precision g measurements and high sensitivity CPT tests.

In the actual development of the experiment, positrons will be accumulated over the course of about 500 sec while antiprotons are being catched and cooled in a magnetic confinement system. A positron bunch is then fired at the converter to produce Ps for the charge exchange reaction. The production process is therefore a pulsed production triggered by the positrons hitting the converter, and by the Ps being laser excited before intersecting the $\overline{p}$ cloud. The antihydrogen production process takes about a microsecond; after that the antiatoms (which would promptly escape the confining magnetic field) are getting accelerated towards the deflectometer by means of a Stark acceleration technique. This strategy has the advantage of avoiding the problem of simultaneously confining charged particles (for ($\overline{H}$ production) and the antihydrogen itself.

The production reaction itself, $Ps^* \, \overline{p} \rightarrow \overline{H}^* e^-$, is one of the key elements of the AEGIS program. This production reaction has been chosen for its favorable cross section, for the possibility of producing antihydrogen in a relatively controlled excitation state and for the possibility to experimentally implement the reaction in such a way that very cold antihydrogen can be formed. This reaction features a strong dependence on the principal quantum number of the Ps state, $\sigma \sim a_0 n^4$ (a_0 being the Bohr radius), whence the requirements for laser excitation of the Ps to high-n (Rydberg) states.

In the first part of this contribution we describe the physics motivation of AEGIS and the experimental method, while in the second part we focus on the more specific topic of laser excitation of Positronium to high-n levels, presenting a theoretical analysis of the Rydberg level structure in strong magnetic fields and specifying the laser pulse characteristics.

2. – The Physics of AEGIS

General Relativity and Quantum Field Theory (QFT) are the very foundation of modern physics. The AEGIS experimental program addresses questions related to both of those fundamental theories: CPT violation and the Weak Equivalence Principle (WEP).

CPT invariance (or CPT theorem) is a flat spacetime symmetry embedded in any modern Quantum Field Theory(QFT); it was proven for the first time by Lüders in 1957 in the frame of lagrangian QFT [2]. The theorem was then given a more general proof

in the frame of axiomatic QFT [3]. In short [4], *any quantum theory formulated on flat spacetime is CPT symmetric provided the theory respects (i) Locality, (ii) Unitarity, (iii) Lorentz invariance*. For these reasons, CPT tests concern the basic foundations of modern quantum theories of particles. Even if CPT invariance seems to be held in all our phenomenology up to now, CPT should break down at some level when Quantum Gravity effects come into play. Quantum Gravity theories are needed when – roughly speaking – the Schwarzschild radius of a particle becomes comparable to its Compton wavelength. This happens at the Planck mass scale $M_P \sim 10^{19}$ GeV or at the Planck length of $l_P \sim 10^{-35}$ m.

The most important consequences of CPT invariance concern the properties of particles and antiparticles, namely that they should have opposite discrete quantum numbers (like charge) and opposite magnetic moments while they should have the same lifetime and inertial mass. Being CPT so fundamental, it is important to test it with the highest possible accuracy using all type of particles: baryons, mesons and leptons.

For lepton systems, the most accurate test is the comparison between the electron and the positron magnetic moments, or gyromagnetic factors, to a precision of 2×10^{-12} [5]. In the baryon sector the charge to mass ratio of protons and antiprotons has been found equal to within 10^{-10} [6]. The meson sector offers the maximal sensitivity being the ratio between the difference of kaon and antikaon masses and their average less than 10^{-18} [7]. The sensitivity of this measurement to CPT–violating parameters is however model dependent [8].

Lorentz–violating extensions of the Standard Model have been considered and parametrized in terms of spacetime operators [9]. Some of the possible terms cause CPT violations and they can be constrained with high accuracy by comparison of hydrogen and antihydrogen spectroscopic properties. The frequency of the 1S–2S transition in hydrogen has a natural linewidth of 10^{-15} (or 1.3 Hz) and it has been measured with an accuracy of $\sim 10^{-14}$ by using a very cold (~ 100 mK) atomic beam [10]. A comparison of the 1S–2S frequency for hydrogen and antihydrogen with similar precision will be the most accurate CPT test ever made for baryons. In addition, an eleventh digit precision in determining the hydrogen and antihydrogen 1S–2S energies yields new information on the equality of the proton and antiproton charge distribution. In fact the theoretical uncertainty is the calculation of the transition energy for the hydrogen atom is in the eleventh digit [11] and is due to uncertainty on the experimental knowledge of the proton radius.

The ground state hyperfine structure (GS–HFS) is another important transition that has been measured in hydrogen with very high (10^{-12}) accuracy. To the leading order, the GS–HFS of antihydrogen is proportional to the spin magnetic moment of the antiproton, which is experimentally known to be equal to the one of the proton only at the 0.3% level [12]. Below the several ppm accuracy, GS–HFS also depends on the electric and magnetic form factors of the antiproton. The measurement of the antihydrogen GS–HFS to a relative accuracy of better than 10^{-6} will therefore yield an improvement on the value of the magnetic moment of the antiproton by three orders of magnitude and give some insight into the structure of the antiproton [11].

The frequency interval between $2S_{1/2}$ and $2P_{1/2}$ states (Lamb shift) originates from QED vacuum polarization and has been measured in hydrogen with 2.7×10^{-6} accuracy. The short lifetime (1.6 ns) of the $2P_{1/2}$ state corresponds to a natural linewidth of 100 MHz which is about 8 orders of magnitude higher than that of the 1S–2S transition. This severely constrains the experimental precision achievable and the power of this transition for accurate CPT tests.

The Weak Equivalence Principle (WEP) is a cornerstone of General Relativity stating that *the trajectories of any falling test particles will be the same in a gravitational field. They will depend only on positions and velocities of the bodies and not on their internal composition.* Given the classical nature of General Relativity the WEP is expected to be violated at some level, when passing from a classical theory to a quantum theory of gravity. Tests of the WEP for matter have been made in the course of the last four centuries. At present, the best sensitivity comes from state-of-the-art rotating torsion balances [13] and from tests of moon and earth acceleration in the solar system (laser lunar ranging [14]). They are both in the range of $\sim 10^{-13}$. On the other side, there have been no direct measurement of the gravitational acceleration of antimatter.

Gravity measurements with charged particles are very difficult because the gravitational force is much smaller than the Coulomb force. Neutral antihydrogen is a unique antimatter system on which the WEP can be directly tested for the first time in a model independent way. A great effort is underway in the attempt to unify all the four interactions and several models leave room for a possible anomalous gravitational behavior for antimatter [15]. A possibility that has generated much interest is that the familiar tensor gravity of our matter world (the spin-2 graviton) might be accompanied by a scalar contribution (a spin-0 graviton) and a vector contribution (a spin-1 graviton) originating forces with opposite sign that happen to cancel for ordinary matter. In such a scenario, the classical potential between two point masses m_1 and m_2 would be of the form:

$$V = -G\, m_1\, m_2\, (1 \pm a\, e^{-r/v} + b\, e^{-r/s})/r \tag{1}$$

with a and b representing the vector and scalar charges and v and s the ranges. Experiments on interactions between matter and matter are sensitive to $\mid a - b \mid$ while for antimatter the sign of a changes so that the experiments are sensitive to the sum $\mid a + b \mid$. Specific models have been in fact constructed where a precise cancelation is takes place for matter–matter interactions [15] while leaving matter–antimatter interaction unconstrained. Using data from Eötvos–like experiments, as well as data from experiments searching for a fifth force limits on the range of scalar and vector fields have been obtained [16] but without excluding the possibility of differential gravitational interaction of matter and antimatter.

Limits on the validity of WEP can be obtained from frequency measurements because the frequency ω of any clock (or $\overline{\omega}$) of an anticlock are linked to the gravitational potential U. This argument requires the validity of CPT, in the sense that $\omega = \overline{\omega}$ when $U = 0$. if CPT is conserved, then a violation of WEP could imply a frequency difference of $\Delta\Omega = \alpha U/c^2$ where α is a parameter describing the violation of WEP.

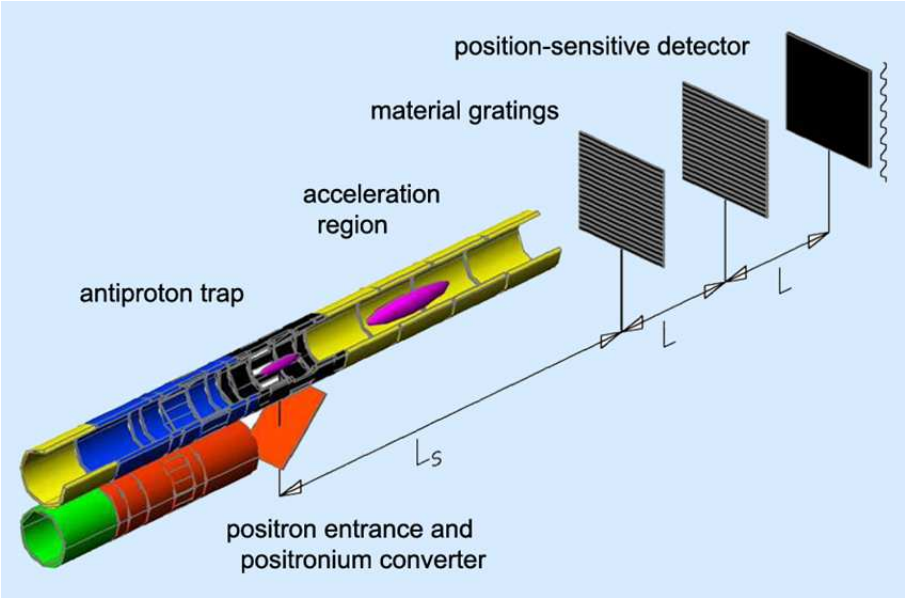

Fig. 1. – Schematics of the central part of the AEGIS experiment (not to scale). Two parallel Penning–Malmberg traps will be used to manipulate the antiprotons and positrons and to form and accelerate antihydrogen. They will be mounted inside a 100 mK cryostat in a 1 T magnetic field. The upper trap is devoted to antiprotons. Cold antiprotons wait for Ps in the black region. The lower trap is devoted to positrons; the positron bunch will be sent on to the converter to produce Ps. Laser pulses will then excite the Ps to Rydberg states to efficiently form antihydrogen in the black region. The yellow region of the upper trap shows the bunch of antihydrogen after the Stark acceleration. Finally, the two material gratings followed by a position sensitive detector for the gravity measurement are shown. Nominal values are $L_s = 30$ cm and $L = 40$ cm. The gratings and detector transverse dimensions are 20×20 cm^2 and the radii of the traps are 8 mm.

3. – The production of the anti–hydrogen beam

In the first phase of AEGIS we will focus on the g measurement performed by means of a hydrogen beam falling in the Earth gravitational field. The most important steps leading to the production of the anti-hydrogen beam are the following:

- Production of positrons in a Surko–type source and accumulator
- Accumulation of the antiprotons from the Antiproton Decelerator
- Production of Ps by positron–bombardment of a porous silica converter
- Laser excitation of the Ps to a $n \simeq 20 - 25$ Rydberg state
- Formation of antihydrogen by means of the reaction $Ps^* \, \overline{p} \rightarrow \overline{H}^* e^-$

- Formation of a $\overline{H}$ beam by Stark acceleration with inhomogeneous electric fields
- Measurement of g in a two–grating Moirè deflectometer coupled with a position-sensitive detector

Fig. 1 shows the central part of the detector. The incoming beam of positrons enters from the lower pipe to hit the converter. Cold antiprotons are residing in the upper electrode pipe which also provides the Stark acceleration to send the antihydrogen beam in the direction of the deflectometer downstream. The last plane of the deflectometer structure will be a position–sensitive microstrip device for the g measurement.

The antiprotons are coming from the CERN Antiproton Decelerator (AD), which delivers about 3×10^7 particles every 100 sec at an energy of 6 MeV. After an energy degrader, antiprotons will be catched in a 3 T magnetic field region (not shown in fig. 1) at a temperature of 4 K. Sympathetic cooling with electrons will take place in this region, before stacking the antiprotons in the hydrogen recombination region. The stacking rate will be of about about $10^4 - 10^5$ antiprotons every 500 sec, in analogy with the to the accumulation time of the positrons.

In the recombination region, schematically shown in fig. 1, there will be an uniform axial magnetic field of 1 T. Penning–Malmberg traps will be used for manipulating charged particles; axial confinement is provided by the electrical potential due to voltages applied to an array of cylindrical electrodes while radial confinement is provided by the magnetic field.

Cooling of the antiprotons here is a key technical element for the realization of the experiment since it will determine the velocity distribution of the antihydrogen. The radial component of the velocity distribution requires particular care since it will determine the number of particles to be geometrically accepted by the Moirè deflectometer downstream, thereby affecting the sensitivity of the g measurement. For antiproton cooling, a design temperature of 100 mK is foreseen, corresponding to a radial velocity of the order of 40 m/s. To achieve this low temperatures for the antiproton cloud resistive cooling based on high-Q resonant circuit techniques are being developed. As an alternative, sympathetic cooling with laser cooled Osmium ions can be employed [17]. The dimensions of the antiproton cloud will be of about 8 mm in the axial and 3 mm in the radial direction.

3˙1. *Ps formation.* – An important part of the experiment is the formation of Ps, an essential ingredient to the antihydrogen formation process. In order to achieve this goal, positrons are produced from a 100 mCi source, moderated, trapped and accumulated during a time period of about 500 sec in a Surko–type device. The final accumulation stage will last about 500 sec to prepare a 20 ns bunch of about 10^8 particles.

The formation of Ps takes place by means of positron bombardment of a nanoporous insulator material (see fig. 2). When e^+ are made to impinge on such materials at a kinetic energy of the order of several keV, they are quickly (in picoseconds) slowed down to energies when Ps formation is energetically feasible, of the order of a few eV. After Ps has been formed in this way and the quickly decaying para–Ps component has died away, the ortho–Ps can be re–emitted into the pore walls. While some of the Ps will be lost

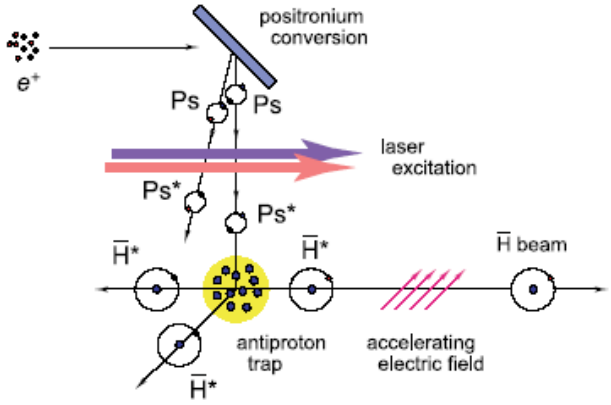

Fig. 2. – Schematics of the antihydrogen production process. The positron bunch lasts about 20 ns while the laser pulse is 5 ns long. The production of antihydrogen will require about 1 μs.

in the pick–off interaction with the e^- of the walls of the pore, the overall effect of Ps bouncing on the pore walls and propagating out of the converter will be one of slowing down and thermalization. Experiments have shown that re-emitted Ps in the amount of about 40% of the impinging e^+ can be obtained in this way [18, 19]. Other measurements as well as preliminary data show that a part of the re–emitted Ps is thermalized down to temperatures of 50 K [20]. We are currently studying the converter material for the experiment, taking into account the overall Ps yield, the level of Ps thermalization (by means of time-of-flight measurements) and the extent to which there characteristics are retained at cryogenic temperatures.

The excitation of Ps to Rydberg states (fig. 2) requires photon energies near the photoionization limit of 6.8 eV, a wavelength too short for commercially available systems. For these reasons we are developing a two–step excitation system that will be described below. Since this laser driven excitation will take place in a 1 T magnetic field, a careful examination of Ps energetics in that situation will be presented. The laser pulse will last about 5 ns, comparable with the duration of the positron bunch (20 ns) and smaller than the characteristic expansion time of the Ps cloud. Roughly, after the excitation, it is estimated that about 30% of the Ps atoms will be excited in a $n \simeq 25$ Rydberg state.

The choice of the best value of the Ps excitation level n will be taken by using the experimental results themselves. Factors that will enter into this choice are: lifetime of the Rydberg levels, dipole–dipole Rydberg interactions, optimization of the Stark acceleration process, maximizing the antihydrogen production rate. The possibility of Ps focusing on the antiproton cloud by means of an electric field gradient is under investigation.

3˙2. *Antihydrogen formation and acceleration.* – The antihydrogen formation will take place through the charge exchange reaction $Ps^* \, \overline{p} \rightarrow \overline{H}^* e^-$ (see fig. 2) that will involve about 10^7 excited Ps atoms and $10^4 - 10^5$ cooled antiprotons. This reaction is of great interest for a series of reason.

First of all, the energy level distribution is reminiscent of the energy levels of the excited Ps; this leads to a relatively limited spread in the energetic of the final system (principal quantum number centered around $n_H \simeq \sqrt{2} n_{Ps}$ and spread of a few units in n). This translates in a lower spread of the velocities following the next step in the experiment (Stark acceleration).

Secondly, the cross section for this reaction ($\sigma \sim 60\,\pi\,a_0^2\,n^4$) has a sharp dependence on the Ps quantum number that could be tuned by means of the laser system. The cross section drops if Ps velocity significantly exceed 10^5 m/s because the center of mass velocity of the reacting system should be lower than the eletron/positron orbital velocity in Ps.

Finally, the antihydrogen formed with antiproton at rest is created with a velocity distribution dominated by the antiproton temperature. Therefore, thanks to the very low antiproton temperature (100 mK, or 40 m/s velocity), the formation of an antihydrogen beam with a limited radial velocity is made possible. This is a significant advance with respect to the rather high antihydrogen temperature observed when using the nested–well technique pioneered by ATRAP [21] and ATHENA [22]. Our approach is conceptually similar to the Cesium-based charged exchange reaction proposed in [23] and successfully demonstrated in ATRAP [24].

As a result of this series of processes and taking into account both the kinetic energy of the antiprotons and the converted internal energy, antihydrogen with an expected velocity of about 50–100 m/s will be produced. Given the numbers of excited Ps atoms and of antiprotons as well as the size of the antiproton cloud (8 mm axial and 3 mm radial dimension) and the relative velocities, it is expected that about 100-1000 antihydrogen atoms will be formed per positron shot on the converter. Since this process will take place after the accumulation on positrons in the positron accumulator and the accumulation and cooling of antiprotons in the catching region, the frequency of the shots will be of about one every 500 sec, translating in an equivalent averaged production rate of a few Hz. The duration of whole process of antihydrogen formation is dominated by the time of flight of Ps ($v \simeq 10^4 - 10^5$ m/s) from the converter to the antiprotons and through the antiproton cloud. This process takes of the order of a μs. The start time is given by the positron accumulator machine delivering the positron bunch to the converter.

After antihydrogen has been created, the acceleration procedure along the beam axis relies on the principle of of the force exerted on a dipole by an electric field gradient. Since the dipole moments scale approximately as n^2, Rydberg atoms are especially suited to being manipulated in this way. The energy levels of an H (anti)atom in an electric field F are given to first order, in atomic units by:

$$E = -\frac{1}{2n^2} + \frac{3}{2} n k F \tag{2}$$

where k is the parabolic quantum number (running from $-(n-1-\mid m \mid)$ to $(n-1-\mid m \mid)$ in steps of two). If the excited atoms are moving in a region where the amplitude of the electric field is changing, then their internal energy changes accordingly (to conserve

total energy). In this way they become accelerated or decelerated. Electric fields of the order of a few 100 V/cm can be used, limited by field ionization of the Rydberg atoms. In this way an acceleration of about 500 m/s can be obtained in about 1 cm. In addition it can be shown [25] that this can be done in such a way as to mildly reduce the radial velocity spread. This technique has been recently demonstrated with ordinary hydrogen after excitation to the $n = 22, 23, 24$ states [26, 27]. In those experiments, accelerations of 2×10^8 m/s have been obtained and a hydrogen beam traveling at 700 m/s has been stopped within 5 μs over a distance of 1.8 mm. In AEGIS we intend to adapt the electron configuration used in these experiments to the geometry of the Penning traps to accelerate antihydrogen in the direction of the deflectometer for the gravity measurement.

Studies of the effect of the 1 T magnetic field have shown that the Stark acceleration mechanism continues to work in a similar way provided the applied electric field is sufficiently perpendicular to the magnetic field, thereby avoiding the chaotic regime.

The time of flight of the antihydrogen after the production point to the end of the deflectometer is of about 5 ms, so that to make the production time ($\sim \mu$s) small and to allow for the decay of most of the Rydberg states down to the fundamental levels. In summary, the antihydrogen atoms will present themselves at the beginning of the deflectometer with an axial velocity of about 500 m/s and a radial velocity spread of about 20 m/s.

4. – The gravity measurement

The gravity measurement involves measuring the fall of a beam flying at an approximate velocity of 500 m/s and having a considerable velocity spread (of the order of $\sigma \simeq 100$ m/s. Given a flight path of about 80 cm, the displacement introduced by gravity is of about $1/2\, g\, t^2 \simeq 35$ μm at $v = 500$ m/s, a quantity that is very difficult to measure, the beam having a spread of about 50 m/s in the vertical direction and an 8 mm spot.

In order to cope with these requirements, the use of a non-dispersive classical Moirè deflectometer is foreseen. The device [28] consists of three equally spaced and parallel material gratings (Fig. 3). In our case, as shown in the figure, the last plane will be made of a position–sensitive microstrip detector to register the impact point of antihydrogen atoms.

As the atomic beam passes through the gratings the first two planes select some propagation directions thereby creating on the third plane a density modulation. This density modulation repeats itself at positions that are integer multiples of the distance between the first two gratings. In addition, the density modulation is independent from the collimation of the incoming atomic beam and has the same periodicity of the first two gratings. This device works therefore as a powerful collimator to enhance the effect of any force acting on the particle. This technique, originally proposed in [29] can be effectively applied to the case of inertial sensing (and gravity measurements) as discussed

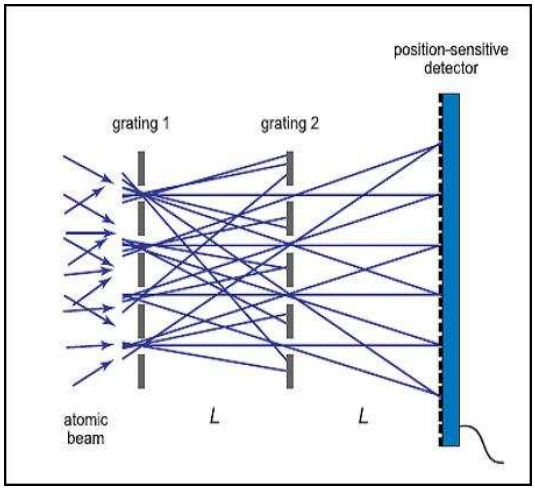

Fig. 3. – Principle of the Moirè deflectometer and the position–sensitive detector for AEGIS. The distance L is 30 cm.

in [28]. For the device to work in the classical regime, it is necessary that:

$$a \gg \sqrt{\lambda_{dB}\, L} \tag{3}$$

where λ_{dB} is the de Broglie wavelength of the particle, a the grating period and L is the spacing between the gratings (30 cm). Under these conditions, the quantum mechanical spread introduced by a grating slit, will not generate a significant shift in the point of impact on the following plane and the whole device still works in a classical regime. These conditions will be met in the nominal case of a grating with a grating period of 80 μm and an opening fraction of 30% (i.e. a 30 μm hole and a 50 μm stopper).

While not relevant to the working principle of the deflectometer, the overall collimation of the beam is still important for our measurement, since an excessive radial velocity will imply that most of the antiatoms will be lost because of the finite acceptance of the device.

When a given number of atoms passes through the detector, the modulation intensity pattern will be shifted by a quantity that depends by the transit time t, the period of the grating and of course g: $\delta = g\,t^2/a$ (fig 4). This means that the fringe shift will depend on the axial velocity of the beam, a quantity that features a considerable spread because of the Stark acceleration mechanism.

In order to detect the gravity effect and to make the measurement of gravity possible, two conditions must be met: the flight time of the antihydrogen will have to be measured on an event-by-event basis and the impact point of the antiatoms of the beam has to be determined with a sufficient spatial accuracy. The impact point of the antihydrogen on the position sensitive detector will be measured by means of a 300 μm thick silicon microstrip detector with a 25 μm pitch. The energy release of the antiproton and the

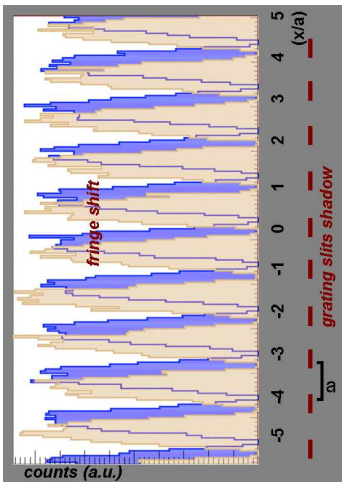

Fig. 4. – Shift of intensity modulation fringes due to the effect of gravity for the case of a grating period of 80 μm, a grating transparency of 30%.

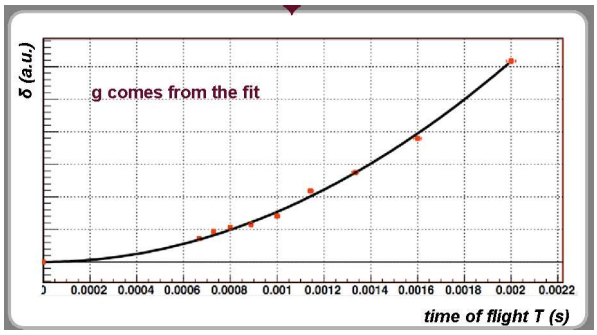

Fig. 5. – Fitting δ as a function of the transit time t to get the gravity constant g according to the expression $\delta = g\,t^2/a$.

consequent nuclear recoil will make possible achieving a resolution of about 12 μm on the impact point. The time-of-flight of the antiatom will be measured by determining the difference between the time of the Stark acceleration pulse and the time of impact of the particle on the microstrip detector downstream.

Since the fringe shift is a function of the particle velocity, g will have to be extracted from a fit where the time-of-flight and the fringe-shift for a given velocity bin are plotted. Fig. 5 shows an example of this fit. Taking into account several possible sources of errors, it has been estimated that a final 1% resolution on g can be achieved by launching 10^5 antihydrogen atoms towards the deflectometer. This will amount to about a month of data taking at the CERN AD.

5. – Positronium laser excitation: theory of Rydberg level structure of moving Ps in strong magnetic fields

The AEGIS experimental program requires the excitation of a Ps cloud to Rydberg levels in a magnetic environment, using a suitable sequence of laser pulses. To ensure a maximal Ps excitation yield within a few nanoseconds (see fig. 2), the characteristics of these pulses in terms of power and spectral bandwidth must be tailored to the geometry, the modified Rydberg level structure and the timing of the Ps expanding cloud, where the single atoms can have random velocities of $10^4 - 10^5$ m/s. Ps Rydberg excitation with nanosecond laser pulses was proposed and experimentally performed in Ref. [30] for n up to 19, but in a different magnetic regime with respect to AEGIS and without

a thorough study of the distribution of interacting Rydberg substates. In this section we present a simple theoretical model describing magnetic interactions acting on moving Ps atoms, while in the following section we determine the laser pulse characteristics, essentially saturation fluence and bandwidth, needed for the goal of maximization of Ps excitation efficiency. A first analysis on this problem was performed in Ref. [31], and some results are reviewed here.

The problem of a compound system of two charged particles moving in an arbitrary magnetic field is a rather complicated one and is still of fundamental interest due to its numerous applications. The behavior of the simpler of these systems, an hydrogen atom in a weak or moderate magnetic field, is a well known topic for experimental investigations and tests on elementary quantum mechanics. Applications of the problem of high magnetic fields is of great interest in astrophysics [32] and in solid-state physics, for instance in the case of an exciton moving in a semiconductor structure [33]. The influence of a strong magnetic field on the high-n states (Rydberg states) of an atom at rest was thoroughly investigated in the past [34, 35], while the more challenging problem of Rydberg states of a *moving* atom in a magnetic field has attracted in the last decade many experimental and theoretical researches [36].

An atom moving in a magnetic field is equivalent to an atom in crossed magnetic and electric fields [37], and this problem has not been completely solved until now. In fact there is no exact analytical solution of the Schrödinger equation of the system in the whole region of values of magnetic field and atom momentum, due to the lack of symmetry. All the theoretical studies of the problem deal with perturbation methods, applicable only in some limiting cases of magnetic field and atom momentum values. Therefore, the energy spectrum and other properties of the system are analyzed mostly in asymptotic regions.

The case of Ps is particularly interesting, because Ps is by far the lightest atom that can be synthesized. Hence the components of its energy spectrum originated by motional effects are of overwhelming importance with respect to similar terms in hydrogen. Studies on Ps in very strong magnetic fields were performed in astrophysics [38], and crossing magnetic and electric fields were considered [39]. But none of these studies focused on the particular modification of the Rydberg levels structure, nor to the optical transitions between them.

We consider a Ps atom in a static magnetic field $\vec{B} = B\hat{z}$; in a perturbative framework the hamiltonian describing the system can be written as:

$$\hat{H} = \hat{H}_C + \hat{H}_F + \hat{H}_Z + \hat{H}_{dia} + \hat{H}_{MS} \tag{4}$$

where the last term on the right side $\hat{H}_{MS}$ represents the proper motional contribution (depending on the center of mass velocity $\vec{v}_{CM}$ [40]), that will be examined in detail later. Here we start our analysis for a Ps at rest in the reference frame of $\vec{B}$ (*i.e.* with $\vec{v}_{CM} = 0$). $\hat{H}_C$ is simply the hamiltonian of a two particle system with opposite electric charges e and $-e$ interacting with the Coulomb potential $e^2/4\pi\varepsilon_0|\vec{r}|$ where $\vec{r}$ is the relative position vector. The second contribution $\hat{H}_F$ represents the fine structure (spin–orbit and spin–

spin relativistic interactions). The third and fourth contributions describe respectively the first order (Zeeman effect) and the second order (diamagnetic or quadratic Zeeman) interaction with $\vec{B}$.

Using the unperturbed atomic quantum numbers n, l, m and the total spin quantum numbers s, m_s, the energy level structure for Ps at rest is then given by the following expression, in which the last term will be added in the case of moving Ps:

$$(5)\ E_{n,l,m,s,m_s} = -\frac{\mu c^2 \alpha^2}{2n^2} + \Delta E_F(n,l,s) + \Delta E_Z(s,m_s) + \Delta E_{dia}(n,l,m)\ \ (+\Delta E_{MS})$$

where μ is the reduced mass (equal to one half of the electron mass) and α the fine structure constant. The first energy term ($= -13.6\,\mathrm{eV}/2n^2$), an eigenvalue of $\hat{H}_C$ with $\psi_{nlm}(\vec{r})$ as a corresponding wavefunction, is a $4n^2$ degenerate manifold with respect to l, m, s, m_s substates. In the Ps case these bare energy levels are exactly 1/2 of the corresponding hydrogenic levels. The expression for the fine structure sublevel energy splitting ΔE_F can be found for example in Ref. [41]; this energy contribution is roughly a factor α^2/n smaller than the bare energy, and turns out to be negligible with respect to magnetic contributions for $n \geq 3$. Therefore, this term will be neglected in the following discussions. In any case the Ps fine structure for $n = 1, 2$ is theoretically and experimentally well known, for its role as a fundamental test on quantum electrodynamics [42, 43]. Let us now discuss the energy contributes originating from magnetic interaction.

5˙1. *Zeeman energy splitting* ΔE_Z. – Defining, as usual, the magnetic dipole momenta associate to orbital angular momentum $\vec{L}$ and spin $\vec{S}$ for both particles, we have $\vec{\mu}_{L(p,e)} = \pm\,(e/2m_e)\,\vec{L}_{p,e}$ and $\vec{\mu}_{S(p,e)} = \pm\,(e/m_e)\,\vec{S}_{p,e}$, where m_e is the electron mass and the gyromagnetic factors are assumed coincident with 2. The explicit expression of the Zeeman hamiltonian ($\mu_B = e\hbar/2m_e$ being the Bohr magneton):

$$(6)\qquad \hat{H}_Z = -\left(\vec{\mu}_{L,p} + \vec{\mu}_{L,e} + \vec{\mu}_{S,p} + \vec{\mu}_{S,e}\right) \cdot \vec{B} = 2\,\mu_B\,B\,\left(S_e^z - S_p^z\right)/\hbar\,,$$

because $\vec{L}_p = \vec{L}_e$ in the center of mass system, canceling the orbital motion terms; hence there is *no energy contribution from magnetic interaction with orbital motion.* We also note that the z–component spin $\hat{H}_Z$ is not diagonal in the singlet (*para*, $s = 0$) and triplet (*ortho*, $s = 1$) basis of Ps states, with spin wavefunctions χ_{s,m_s} [44]. In fact the matrix element $< \chi_{s',m'_s}|S_e^z - S_p^z|\chi_{s,m_s} >$ is nonzero only when $m'_s = m_s = 0$ and $s' \neq s$, so that the magnetic perturbation only mixes these ortho and para states, while the $m_s = \pm 1$ states remain unaffected. The Zeeman energy splitting involves only $m_s = 0$ substates, and its maximum value can be evaluated as $\Delta E_Z = 4\mu_B B$. For the reference field of $B = 1$ T, this amount to 2.4×10^{-4} eV, which in fact is very small with respect to the motional splitting of Rydberg substates, as discussed later.

The level mixing leads to the well known enhancement of the average annihilation rate of the Ps thermal ground state $n = 1$ (*magnetic quenching*) [42, 44], leaving in fact only the unperturbed ortho–Ps states with $m_s = \pm 1$ surviving in the Ps cloud expanding from the positron converter. From the observation that the electric dipole selection rules for

optical transitions impose conservation of spin quantum numbers, we may conclude that in first approximation the Zeeman effect does not play any role in the laser excitation.

5˙2. *Diamagnetic energy splitting* ΔE_{dia}. – The hamiltonian of the quadratic Zeeman effect is $\hat{H}_{dia} = (e^2/8\mu)\left(\vec{r}\times\vec{B}\right)^2$ and has nonzero matrix elements if $\Delta l = 0, \pm 2$ and every Δn; it turns out that one has some mixing of n, l levels for very high fields ($B > 10^2$ T). The first order energy shift is $\Delta E_{dia}(n,l,m) =< \psi_{nlm}|\hat{H}_{dia}|\psi_{nlm} >= (e^2B^2a_{Ps}^2/8\mu)\, f(n,l,m)$, where a_{Ps} is the Ps Bohr radius ($a_{Ps} = 2a_0$). The numerical factor $f(n,l,m)$ is a sum of a n–dependent positive contribute and a l, m splitting term, both proportional to n^4 [45, 34]. Hence one has an energy correction to high-n energy bare levels, but for Ps this is relevant only for $n > 40$, leading to an enhanced ionization probability. The energy splitting of n–substates, whose maximum value is ΔE_{dia}, turns out to be of the same order of ΔE_Z for the n values of interest for laser excitation (see Fig. 6).

5˙3. *Motional Stark (MS) energy splitting* ΔE_{MS}. – Finally we discuss the energy contribution ΔE_{MS} arising from the motional hamiltonian $\hat{H}_{MS}$, that has to be added to the other energy terms in eq. (5) in the case of a moving Ps. An approximate expression for $\hat{H}_{MS}$ can be found by relaxing the assumption of Ps atom at rest. If a Ps atom is moving with center of mass velocity $\vec{v}_{CM}$ in the reference frame of the static B field (in which the electric field $\vec{E} = 0$), the transformed fields in Ps rest frame (to the first order in $\vec{v}_{CM}/c$), are given by:

$$\vec{B}' = \vec{B}\,; \qquad \vec{E}' = \vec{v}_{CM}\times\vec{B} \equiv \vec{E}_\perp\,. \tag{7}$$

Therefore an induced transverse electric field $\vec{E}_\perp$ is acting on the moving Ps, and the relative hamiltonian is easily written as a Stark hamiltonian [46]:

$$\hat{H}_{MS} = -e\,\vec{r}\cdot\vec{E}_\perp = -e\,\vec{r}\cdot\left(\vec{v}_{CM}\times\vec{B}\right), \tag{8}$$

justifying calling this phenomenon as a *motional Stark effect*. This formula can also be derived, with some assumptions, from a more formal analysis of the problem of two charged particles moving in arbitrary B field [40].

A moving Ps atom is therefore interacting with crossed $\vec{B}$ and $\vec{E}$ fields; in this case one has complete breaking of the original axial symmetry around the $\vec{B}$ axis, with the consequence that the matrix elements of $\hat{H}_{MS}$ are different from zero every Δl and Δm. There is *a complete mixing of l and m substates* belonging to the same n manifold (the mixing between bare n states does not occur to a good extent [47]). Hence l, m are no longer good quantum numbers labelling the substates (and no other quantum number is known for this problem!), differently than the principal quantum number n which retains its role [46, 30]. Note also that the electric dipole selection rules for optical transition lose any significance and any mixed substate can be excited from ground using a suitable electromagnetic radiation.

We can evaluate the maximum energy splitting ΔE_{MS} between the n^2 sublevels of an opened n–fan from the usual theory of the Stark effect, obtaining:

$$\Delta E_{MS} \,=\, 3\, e\, a_{Ps}\, n\,(n-1)\;|\vec{E}_{\perp})| \,=\, 3\, e\, a_{Ps}\, n\,(n-1)\; B\, v_{\perp}\,, \tag{9}$$

where we will consider $v_{\perp} = \sqrt{k_B T/2m_e}$ for the transverse component of Ps thermal center of mass velocity (T being the temperature of the Ps cloud). The energy ΔE_{MS} increases both with B and n and, because Ps is nearly 1000 times lighter than hydrogen, the MS field has some important and previously unnoticed effects [31].

At a reference temperature of 100 K and a magnetic field of 1 T, one has $v_{\perp} \approx 2.8{\times}10^4$ m/s and an induced electric field $E_{\perp} \approx 275$ V/cm. With such an high field the possibility of Rydberg Ps ionization has to be considered: the transition from the bound state to an ionized state occurs from the bottom sub–level of an opened n–fan (the *red–state*) to the unbound states. The minimum Stark electric field which induces high ionization probability on the sublevel with the lowest energy is calculated as $|\vec{E}_{min}| = (e/4\pi\varepsilon_0 a_{Ps}^2)\,(1/9\,n^4)$ [47]. Hence the ionization starts affecting part of the n–sublevels for $n > 27$, which constitutes a limit for any attempt to Rydberg state excitation. Note that in the case of hydrogen, $v_{\perp}$ and $E_{\perp}$ are a factor 1/30 smaller with respect to Ps, and the ionization starts at $n > 87$. Moreover it is easy to see that in hydrogen the motional splitting remains lower than ΔE_Z or ΔE_{dia} for low n or high n, respectively, while in Ps the energy splitting ΔE_{MS} rapidly becomes dominant over the other splittings for $n > 6$ (see Fig. 6).

However the most impressive property of the Rydberg substates reorganization under the MS effect is the following. The energy distance between neighboring bare n levels decreases as $\Delta E_n \,\simeq\, 13.6\,\mathrm{eV}/n^3$. Therefore when $n > 17$ the bandwidth filled by the MS sublevels relative to an n state becomes overwhelmingly greater than the interval between two adjacent n–levels. Thus, at n larger than 17 *an interleaving of many n–sublevel manifolds* is expected, leading to an apparent full mixing of n, l, m states. Note that the range of n levels useful for the charge transfer reaction and efficient $\overline{H}$ formation in AEGIS starts from $n \sim 20$, *i.e.* in this region of notable level mixing.

Fig. 6 summarizes the results on the different magnetic contributes to n–sublevels splitting; it is clear that the MS effect dictates the Rydberg structure in Ps; also indicated are the two regions of level mixing and the ionization limit. A schematic illustration of the n–sublevels interleaving phenomenon, as a function of the induced Stark electric field (proportional to magnetic field or to the square root of temperature), is shown in Fig. 7. The unusual distribution of sublevels raises questions about optical resonances and line broadenings, that we will consider in the next Section. Finally, in Figs. 9 and 10 we plot the ionization limit and the value of the n separating the regions of simple l, m mixing and of full n, l, m mixing, as a function of T and B respectively. One can observe that the position and the extension of the complete mixing region are weakly dependent on these parameters, hence our discussion on the properties of a single Ps atom retains its validity also by considering an ensemble of Ps atoms with a velocity distribution, as happens in the Ps cloud exiting the converter.

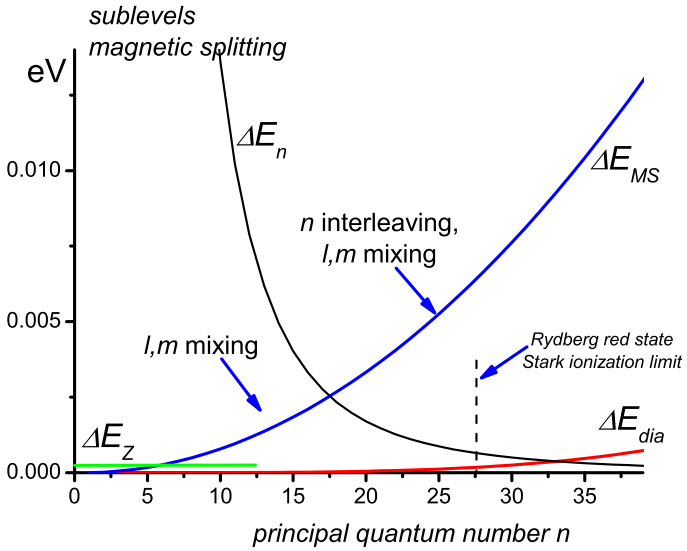

Fig. 6. – The three magnetic contributions to the n–sublevels splitting for Ps, as a function of n, for the reference temperature and magnetic field of 100 K and 1 T, respectively. The curve ΔE_n represent the energy distance between neighboring n unperturbed states.

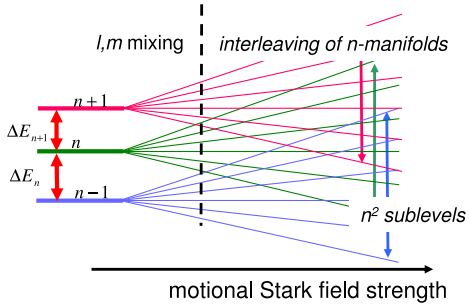

Fig. 7. – Schematic of l, m mixing and n–sublevels interleaving.

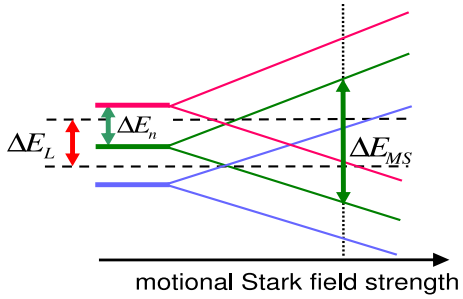

Fig. 8. – Schematic of the mixing with respect to the laser energy bandwidth ΔE_L.

6. – Positronium laser excitation: tailoring pulse energies and bandwidth

Laser excitation of Ps to Rydberg levels involves wavelengths of about 180 nm. Since this does not correspond to commercially available systems, in AEGIS a two–step excitation with two simultaneous laser pulses was proposed. Two different strategies are possible: (1) from ground state to $n = 2$ and then to high–n levels (partially tested in an experiment in low magnetic field [30]), and (2) from ground state to $n = 3$ and then to high–n levels; the corresponding excitation wavelength are listed in Tab. I). This second choice was proposed because the intermediate level $n = 2$ has a three times shorter

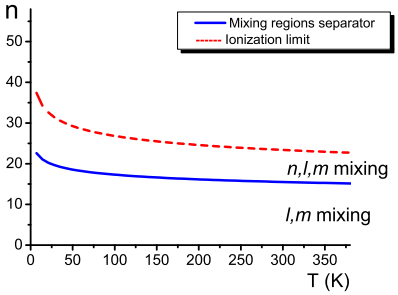

Fig. 9. – The ionization limit and the different mixing regions versus temperature.

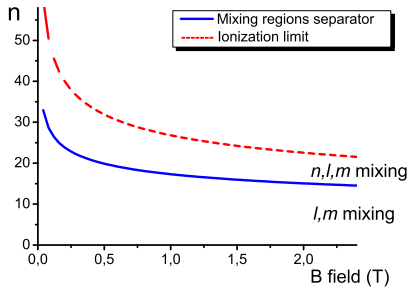

Fig. 10. – The ionization limit and the different mixing regions versus magnetic field.

lifetime than the the $n = 3$ level (3 ns versus 10.5 ns), hence population loss can be dynamically relevant in the excitation. In this Section we determine the laser pulse characteristics tailored to the structure of Rydberg levels in moving Ps atoms, having in mind the goal of maximizing the excitation efficiency.

In an ensemble of moving atoms, all optical resonances are broadened by *Doppler effect*: the resonance frequency of a transition depends (to first order in v/c) on the atom velocity as $\omega = \omega_0 (1 + v_\parallel/c)$, where ω_0 is the resonance at rest and $v_\parallel$ the component of velocity parallel to the propagation direction of the laser field. Assuming a Maxwellian thermal distribution of Ps atoms velocity, the fraction of atoms resonant at ω is:

$$\frac{N_{Ps}(\omega)}{N_{Ps}} = \frac{1}{\Delta\omega\,\pi} \exp\left(-\frac{(\omega-\omega_0)^2}{\Delta\omega^2}\right) \equiv g_D(\omega-\omega_0)\,, \tag{10}$$

where $\Delta\omega = \omega_0\sqrt{2k_BT/mc^2}$ and $g_D(\omega)$ represents the normalized spectral lineshape of the Doppler effect. For high excitation efficiency the laser bandwidth has to cover the lineshape of the resonance; this means that we must consider two broad linewidths, one associated to Doppler effect and the other associated to the MS effect, which is the dominant source of resonance broadening for moving Ps in magnetic field.

The spectral profile of the two laser intensities is commonly characterized by a Gaussian function whose full width at half maximum (FWHM) is $\Delta\lambda_L$. Laser pulses with broad laser linewidths have a low phase coherence, which can be characterized by the coherence time $\Delta t_{coh} = \lambda^2/c\,\Delta\lambda_L$, where $\lambda = 2\pi c/\omega_0$. This parameter turns out to be up to three orders of magnitude shorter than the average 5 ns duration of the laser pulses [1], hence we are operating with a completely incoherent excitation. In this case, with sufficiently high laser power to saturate the transition, and neglecting any decay processes like spontaneous emission, the maximum efficiency in excitation is 50%, corresponding to population equally distributed on interacting levels.

To calculate the energy and bandwidth of the laser pulses necessary for saturation of the proposed transitions, we consider the theory of incoherent excitations [48]. The

Table I. – *Wavelength of the different transition for both excitation paths, with associated Doppler and motional Stark linewidth in nm, for the reference $T = 100$ K and $B = 1$ T.*

	λ	$\Delta\lambda_D$	$\Delta\lambda_{MS}$
$1 \to 2$	243	0.054	$0.85 \cdot 10^{-3}$
$2 \to n > 15$	730	0.16	> 0.9

	λ	$\Delta\lambda_D$	$\Delta\lambda_{MS}$
$1 \to 3$	205	0.045	$1.8 \cdot 10^{-3}$
$3 \to n > 15$	1650	0.36	> 4.0

excitation probability for unit time of level b starting from level a is:

$$W_{a\to b}(t) \;=\; \int_{\Delta E_L} d\omega\, \frac{I(\omega,t)}{\hbar\,\omega}\; \sigma_{ab}(\omega) \tag{11}$$

where $I(\omega,t)$ is the spectral radiation intensity with energy bandwidth $\Delta E_L = \Delta\lambda_L\, hc/\lambda^2$. The photon absorption cross section σ_{ab} is given by

$$\sigma_{ab}(\omega) \;=\; \hbar\,\omega\, g(\omega-\omega_{ab})\, B_{a\to b}(\omega)\,/\,c\,. \tag{12}$$

where the function $g(\omega-\omega_{ab})$ is a normalized transition lineshape. The factor $B_{a\to b}(\omega)$ is the absorption Einstein coefficient appropriate to the dipole–allowed transition. In first approximation [46] this coefficient coincides with that of unperturbed transitions, and one has $B_{a\to b}(\omega) = |d_{a\to b}|^2\pi/\varepsilon_0\hbar^2$, with the electric dipole matrix element $d_{a\to b} = \langle\psi_b|e\,\vec{r}\cdot\vec{\epsilon}|\psi_a\rangle$ ($\vec{\epsilon}$ being the radiation polarization vector) calculated using standard methods from the general theory of radiative transitions in atomic physics [49]. From the excitation probability, and choosing a suitable laser bandwidth (see later), it is possible to derive an expression for the *saturation fluence* $F_{sat}(a \to b)$, a reference parameter characterizing laser power, defined asthe total pulse energy for unit target area which with we obtain 43% of the atoms in the excited state. This conventional value comes from deriving the saturation fluence from simple rate equations (see the Appendix).

Now we apply the theory of incoherent excitations to our selected transitions. We start with an analysis of the broadening of optical transitions, for both the proposed excitation paths. A calculation of the Doppler linewidth $\Delta\lambda_D = \Delta\omega\,\lambda^2\sqrt{\ln 2}/\pi c$ and of the MS width $\Delta\lambda_{MS} = \Delta E_{MS}\,\lambda^2/hc$ gives the values listed in Tab. I.

It is clear that for the first step (excitation to low n) the dominant contribution to the line broadening comes from the Doppler effect, while for the second step (excitation to Rydberg levels) the MS effect largely dominates. Therefore we will consider the two cases separately. Note that both contributions to excitation line broadening depend on the square root of T (being proportional to Ps velocity), hence one expects that the following discussion on transitions and laser pulse characteristics is not qualitatively affected by changing the temperature of Ps cloud.

6˙1. *Fluence of laser pulses for low n excitations.* – In this case, assuming for definiteness (from now on) a linear laser polarization parallel to the magnetic field axis, we have an unperturbed transition between hydrogenic states $(1,0,0)$ and $(n,1,0)$ with

$n = 2, 3$. The saturation fluence can be easily calculated from the rate equation theory in Appendix, by matching the resonant laser linewidth $\Delta\lambda_L$ to the Doppler broadening $\Delta\lambda_D$ (and using g_D in eq. (12)), to the aim of maximizing the overlap in the spectral domain. We arrive at the result:

$$F_{sat}(1 \to 2,3) = \frac{c^2}{B_{1\to 2,3}} \sqrt{\frac{2\,\pi^3}{\ln 2}} \cdot \left(\frac{\Delta\lambda_D}{\lambda^2}\right)_{2,3} . \tag{13}$$

This formula gives the lowest pulse fluence needed for reaching transition saturation, and is proportional to the selected bandwidth, as expected. From this formula it is easy to determine the laser pulse energy, depending on the target spot size, as discussed later.

6˙2. *Fluence of laser pulses for Rydberg level excitations.* – The physics of the second transition $n = 2, 3 \to$ high–n is significantly different from the simple Doppler–dominated first transition. As depicted in Fig. 11 (for excitation starting from $n = 3$, taken as a reference in the following) the Doppler broadening is practically independent from n, whereas the MS broadening turns out to be many times higher. In the previous Section we investigated the properties of the n^2 sublevels fan distributed in $\Delta\lambda_{MS}$: all sublevels originate from a full mixing of unperturbed hydrogenic levels, and can interact with radiation because of lacking of validity of dipole selection rules. Moreover in the AEGIS useful n–range there is an interleaving of different n–manifolds. Thus one can expect a rapid growth of the saturation fluence, with a consequent very high energy requirement on laser pulses.

In order to derive an expression for the second step saturation fluence, we observe that in practice the huge number of sublevels in $\Delta\lambda_{MS}$ can be considered as a quasi–continuum of energy levels (a Rydberg level band); hence we introduce the *density of energy levels per unit angular frequency* $\rho(\omega)$ [31]. Assuming an energy uniform distribution of the sublevels in the full mixed range, this quantity can be evaluated by dividing the number of interleaved unperturbed n bare levels under the MS energy width times the n^2 multiplicity, by the width itself:

$$\rho(\omega) \;=\; \frac{n^2\,\Delta E_{MS}/\Delta E_n}{\Delta E_{MS}/\hbar} \;=\; n^5\,\frac{\hbar}{13.6\;eV} \; . \tag{14}$$

It is worth noting that $\rho(\omega)$ is independent from the induced Stark field and consequently from the Ps velocity and on B. We stress that this result occurs with a MS effect high enough for producing an interleaving of many n-level fans, and it increases very quickly with n. Within the uninteresting region of the transitions up to $n < 17$ it is easy to see that the density of sublevels is a constant on n.

In the spirit of an optical excitation of a level band, we select the laser energy bandwidth ΔE_L to be smaller than ΔE_{MS} for constraining Ps excitation within a reasonable narrow energy band (seemingly suitable for an efficient charge transfer reaction), but greater than Doppler broadening for Ps cloud efficient spectral coverage. Generalizing

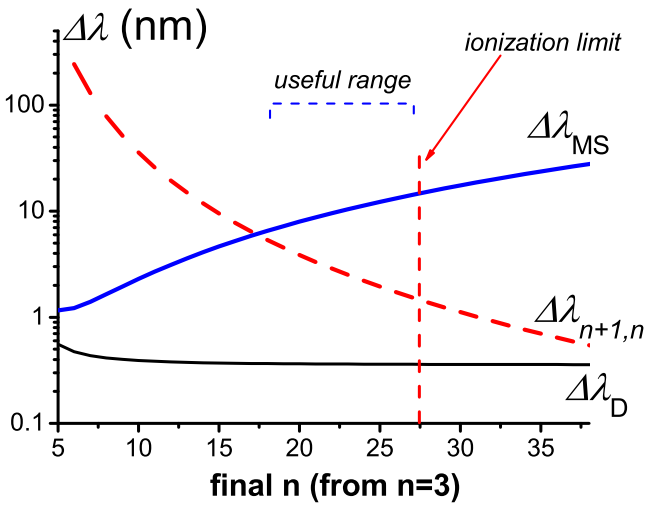

Fig. 11. – Comparison between Doppler and motional Stark broadening for Rydberg level optical excitations. $\Delta\lambda_{n+1,n}$ is the distance (in nm) between neighboring unperturbed n states. The ionization limit and the AEGIS useful range are indicated.

the theory of incoherent excitations, we recast the absorption cross section in eq. (12) as:

$$\sigma_{3n}(\omega) \;=\; \hbar\,\omega\,\rho(\omega)\,B_{MS}(\omega)\,/\,c\,, \tag{15}$$

with the absorption coefficient $B_{MS}(\omega)$ appropriate for the excitation of a single sublevel of the quasi–continuum Rydberg level band. By definition this coefficient must be proportional to the square modulus of the electric dipole matrix element $|\langle\psi_{n\alpha}|e\,\vec{r}\cdot\vec{\epsilon}\,|\psi_{310}\rangle|^2$ where $\psi_{n\alpha}$ is the wavefunction of a sublevel. The following considerations allows us to estimate the magnitude of B_{MS}. The wavefunction $\psi_{n\alpha}$ can be expanded in a linear superposition of the n^2 unperturbed hydrogenic wavefunctions $\psi_{n\alpha} = \sum_{lm} c_{lm}\,\psi_{nlm}$. From the normalization condition and assuming a large spreading of $\psi_{n\alpha}$ over the ψ_{nlm}, we get $|c_{lm}| \simeq 1/n$. Using the electric dipole selection rules, which select the final state nlm, we obtain a simple formula connecting B_{MS} with the absorption Einstein coefficient for the unperturbed $3 \to$ high–n transition:

$$B_{MS}(\omega) \propto \frac{1}{n^2}\,|\langle\psi_{nlm}|e\,\vec{r}\cdot\vec{\epsilon}\,|\psi_{310}\rangle|^2 \quad\Rightarrow\quad B_{MS}(\omega) \simeq \frac{1}{n^2}\,B_{3\to n}(\omega)\;. \tag{16}$$

Note that, because the normalized Rydberg state wavefunctions scale as $n^{-3/2}$ [47], the Einstein coefficient scales as n^{-3} and $B_{MS} \propto 1/n^5$. The absorption probability $W_{3\to n}$ defined in eq. (11) is an integral containing B_{MS} and $\rho(\omega)$; therefore this result

brings about the noteworthy conclusion that *the absorption probability is practically independent of n and of the transverse Ps velocity* [31]. This statement, strictly linked to the interleaving of n–manifolds, can be intuitively understood with the help of Fig. 8. The number of interacting levels per unit bandwidth remains, in a crude approximation, unchanged with the increase of the fan aperture because the sublevels lost at the border of the initially chosen laser bandwidth ΔE_L are compensated by the arrival of sublevels coming from the nearby n-states. In this view it is also clear that the precise bandwidth selection is of scarce importance for these transitions.

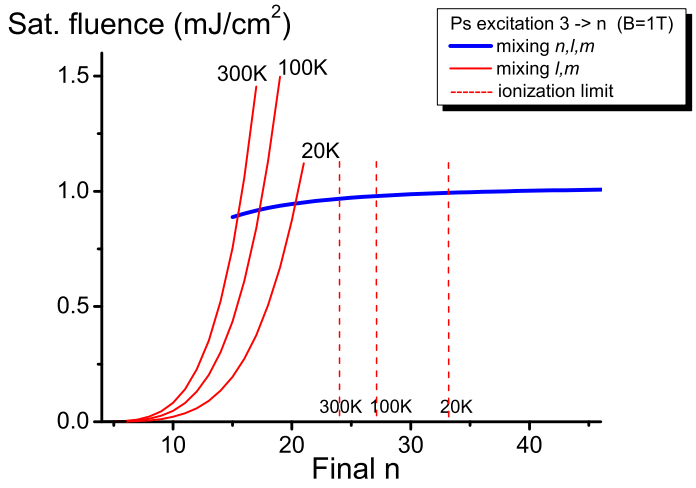

Fig. 12. – The saturation fluence for Rydberg band transitions $3 \to n$ calculated for three different temperatures. The ionization limit is indicated.

Finally, Using eqs. (14) and (16), and following the procedure outlined in the Appendix, we obtain this formula for the Rydberg band saturation fluence:

$$F_{sat}(2,3 \to n) \simeq \frac{c \times 13.6\,\mathrm{eV}}{B_{2,3\to n}\,\hbar\, n^3}\ , \tag{17}$$

which, as expected, is approximately a constant in the full mixing range. In Fig. 12 we plot $F_{sat}(3 \to n)$ for some temperatures. The saturation fluence is rapidly growing in the region of simple l, m mixing, but flattens off nearly to a constant value in the full mixing region. Note that the ionization limit gets lower as a function of T, restricting the useful region for Rydberg excitation.

6˙3. *Laser pulse energies and excitation efficiency.* – From the data on F_{sat}, we can calculate laser pulse energies by assuming pulses with transverse Gaussian profile. We consider a spot size overlapping a Ps cloud of FWHM dimension $\Delta r \approx 2.8$ mm, and fix the

Table II. – *Energies of laser pulses resonant with the selected transitions, for both excitation paths. Calculations are for the reference $T = 100\ K$ and $B = 1\ T$.*

	λ	pulse energy
$1 \rightarrow 2$	243	4.4 μJ
$2 \rightarrow 25$	730	1.5 mJ

	λ	pulse energy
$1 \rightarrow 3$	205	32 μJ
$3 \rightarrow 25$	1664	350 μJ

fluence at the peak of transverse profile as $F_{max} = 4F_{sat}$, to saturate the transitions and retain a security factor for maximum excitation. The laser bandwidth is selected as equal to Doppler bandwidth for all transitions. The results, for both excitation paths and for the case of excitation towards $n = 25$, are summarized in Tab. II. The required energies are well in the range of existing laser facilities, or can be reached with amplifications stages; in the AEGIS proposal a list of possible solutions can be found.

It is important to evaluate the excitation efficiency. The real Rydberg excitation is performed with near simultaneous laser pulses, because of the narrow useful time window to cope with a rather large expanding Ps cloud, and the need of avoiding losses on intermediate level populations due to non negligible spontaneous emission. The incoherent excitation dynamics involves all the three levels of the two–step transition. With the above pulse energies, satisfying transitions saturation, an overall level population of 33% is therefore expected, in the limit case of no losses. This can be confirmed by a dynamical study of the excitation processes, performed in Ref. [31] with a suitable model based on Bloch equations, and including population losses due to spontaneous decay and photoionization. Inserting losses is necessary for a correct description of the dynamics of Rydberg level populations, because these processes are in competition with Rydberg excitation, and in fact ionization processes can be responsible for the overwhelming majority of the population loss rate.

Since the laser pulses are substantially incoherent, the light phase in the dynamical model is taken as a "random walk" with the step equal to the coherence time. Therefore the final excitation probability for Ps excitation comes from an averaging process over many simulation outputs. The calculation shows that a fraction of about 25% of Ps atoms are excited to Rydberg states using the path $1 \rightarrow 2 \rightarrow 25$, while the larger fraction of 30% is excited using the alternative $1 \rightarrow 3 \rightarrow 25$. The difference is mainly due to the higher $n = 2$ spontaneous decay rate and Doppler linewidth (with respect to $n = 3$), with an increase in population losses and in incoherent excitation dynamics, with the result of a reduction in average excitation efficiency.

7. – Conclusions

We have presented an experiment for the measurement of the gravitational acceleration of antimatter, discussing in particular an essential part of it, the Ps laser excitation. The AEGIS design is based upon on a series of ongoing tests and developments (charge exchange production of $\overline{H}$, Stark acceleration and propagation through the Moire de-

flectometer, resolution of the position–sensitive detector). The proposed gravity measurement becomes feasible by merging in a single experimental apparatus technologies already demonstrated and including some reasonable additional development. The proposed design of the apparatus is modular and readily allows, in a future stage, the insertion of a magnetic trap for $\overline{H}$, which will be spatially separated from the region where the antiatoms are produced. The spatial separation between the production and measurement regions differs significantly from the approach chosen by other experiments like ATRAP [21], which incorporates a trap that simultaneously confines charged and neutral particles. A trapped bunch of $\overline{H}$ can be laser–cooled to mK temperatures, at which spectroscopic CPT tests with a sensitivity competitive with current limits on CPT violations become feasible.

An essential part of the AEGIS design is the production of a cloud of Ps atoms and their excitation to Rydberg levels by suitable laser pulses. This process happens in a strong magnetic field, inducing a complete reorganization of the energy level structure. The MS effect splits and totally mixes the otherwise degenerate sublevels of Rydberg states, and totally overcomes the Doppler effect in determining the bandwidth of the transition, as demonstrated by a careful perturbative analysis of various magnetic effects acting on a moving Ps. An important consequence of the MS effect is that the range of high-n levels on which one can obtain high excitation efficiency is limited because Ps atoms are easily ionized by the induced electric field. It must be further researched how this can affect the efficiency of the charge exchange reaction for $\overline{H}$ production, which requires very high-n excitation levels.

Simple considerations based on the general theory of radiative transition in atomic physics are used to derive rules which give the laser pulse fluence, the power and the bandwidth required for the saturation of the transition. The results are tested with numerical experiments, and foresee an efficiency around 30% for an excitation path based on the two–step transition $1 \to 3 \to n$. Anyway, a refinement of the incoherent excitation theory and a realistic modelization of excitation dynamics can help in understanding the processes involved, and in optimizing the experimental design.

Appendix A.

Definition of saturation fluence

The dynamics of incoherent excitation by a laser pulse can be described by a rate equation model [48]. Considering a dipole allowed transition between single states $a \to b$ and neglecting spontaneous emission, the rate equation for the high level population is:

$$\frac{dP_b}{dt} = -P_b\, W_{b\to a}(t) + P_a\, W_{a\to b}(t) \tag{A.1}$$

where $W_{b\to a}$ and $W_{a\to b}$ (defined in eq. (11)) are time–dependent probabilities of induced emission and absorption, respectively. In this simple process, one has conservation of total population $P_a + P_b = 1$ and, from Einstein relations, the relation $W_{b\to a} = W_{a\to b}$.

The excitation is performed with a resonant laser pulse having a total intensity $I_L(t) = \int_{\Delta E_L} d\omega\, I(\omega, t)$, where $I(\omega, t)$ is taken as a time–dependent Gaussian spectral intensity, for simplicity.

In the case of a Doppler dominated transition, the laser broadening is selected equal to the Doppler broadening (as discussed in Section 3.1). Using the fact that the absorption coefficient $B_{a\to b}$ of eq. (12) is in practice a constant, depending only on quantum numbers, the rate equation (A.1) can easily be solved with initial condition $P_b(0) = 0$ obtaining:

$$2\, P_b(t) \;=\; \left[1 - e^{-2F(t)/F_{sat}}\right] , \tag{A.2}$$

where $F(t) \;=\; \int_{-\infty}^{t} dt'\, I_L(t')$ is the laser pulse fluence, and

$$F_{sat}(a \to b) \;=\; \frac{c\sqrt{2}}{B_{a\to b}\, g_D(0)} \tag{A.3}$$

defines the saturation fluence. This parameter characterizes the population dynamics: when $F(t) = F_{sat}$ we have 43% of the atoms in the excited state. The excitation yield can reach 50% with high enough pulse energy.

In the case of MS dominated transitions, a similar calculation is performed without reference to a specific bandwidth and using eq. (15). The saturation fluence is then given by eq. (17).

* * *

We thank the organizers of the School for their kind invitation. We acknowledge several useful discussions with S.Cialdi, I.Boscolo, D.Comparat and F.Villa.

REFERENCES

[1] Kellerbauer A. et al., *Nuclear Instr. & Methods B*, **266** (2008) 351.
[2] Lüders G., *Ann. Phys.*, **2** (1957) 1.
[3] Jost R., *Helvetica Phys. Acta*, **30** (1957) 409.
[4] Mavromatos N.E., invited talk at *International Conference on Exotic Atoms*, published by the Austrian Academy of Sciences, Vienna 2005.
[5] Van Dyck Jr. R.S., Schwinberg P.B. and Dehmelt H.G., *Phys. Rev. Lett.*, **59** (1987) 26.
[6] Gabrielse G. et al., *Phys. Rev. Lett.*, **82** (1999) 3198.
[7] Particle Data Group, *Phys. Lett. B*, **667** (2008) 1.
[8] Hayakawa M., Proceedings of the *First KEK meeting on CP violation and its origin*, **193**, hep-ph/9704418.
[9] Kostelecky M., *http://www.physics.indiana.edu/∼kostelec/*.
[10] Niering M. et al., *Phys. Rev. Lett.*, **84** (2000) 5496.
[11] Sapirstein J.R. and Yennie D.R, *Theory of hydrogenic bound states* in "Quantum Electrodynamics", edited by Kinoshita T. (World Scientific, Singapore) 1990.
[12] Pask T. et al., *Phys. Lett. B*, **678** (2009) 55.
[13] Schlamminger S. et al., *Phys. Rev. Lett.*, **100** (2008) 041101.

[14] Williams J.G. et al., *Phys. Rev. Lett.*, **93** (2004) 261101.
[15] Nieto M.M. and Goldman T., *Phys. Rep.*, **205** (1991) 221.
[16] Bellucci S. and Faraoni V., *Phys. Rev. D*, **49** (1994) 2922.
[17] Warring U. et al., *Phys. Rev. Lett.*, **102** (2009) 043001.
[18] Liszkay L. et al., *Applied Phys. Lett.*, **92** (2008) 063114.
[19] Brusa R., *This conference*
[20] Charlton M., *Phys. Lett. A*, **143** (1990) 143.
[21] Gabrielse G. et al., *Phys. Rev. Lett.*, **93** (2004) 073401.
[22] Madsen N. et al., *Phys. Rev. Lett.*, **94** (2005) 033403.
[23] Hessels E.A. et al., *Phys. Rev. A*, **57** (1998) 1668.
[24] Storry C.H. et al., *Phys. Rev. Lett.*, **93** (2004) 263401.
[25] Testera G. et al., *Pbar08 - Workshop on Cold Antimatter Plasmas and Application to Fundamental Physics, Okinawa, Japan, 2008.*
[26] Vliegen E. and F. Merkt, *J. Phys. B*, **39** (2006) L241.
[27] Vliegen E. et al., *Phys. Rev. A*, **76** (2007) 023405.
[28] M.K. Oberthaler et al., *Phys. Rev. A*, **54** (1996) 3165.
[29] O. Kafri, *Optics Letters*, **5** (1980) 555.
[30] Ziock K.P., Howell R.H., Magnotta F., Failor R.A. and Jones K.M., *Phys. Rev. Lett.*, **64** (1990) 2366.
[31] Castelli F., Boscolo I., Cialdi S., Giammarchi M.G. and Comparat D., *Phys. Rev. A*, **78** (2008) 052512.
[32] Fassbinder P. and Shweizer W., *Astron. Astrophys.*, **314** (1996) 700; Pavlov G.G. and Meszaros P., *Astrophys. J.*, **416** (1993) 752.
[33] Lozovik Yu.E., Ovchinnikov I.V., Volkov S.Yu., Butov L.V. and Chemla S.D., *Phys. Rev. B*, **65** (2002) 235304.
[34] Garstang H., *Rep. Prog. Phys.*, **40** (1977) 8.
[35] Wunner G. and Ruder H., *Phys. Scr.*, **36** (1987) 291.
[36] Wiebusch G., Main J., Krüger K., Rottke H., Holle A. and Welge K.H., *Phys. Rev. Lett.*, **62** (1989) 2821; Main J., Schwacke M. and Wunner G., *Phys. Rev. A*, **57** (1998) 1149; Lozovik Yu.E. and Volkov S.Yu., *Phys. Rev. A*, **70** (2004) 023410, and references therein.
[37] Gor'kov L.P. and Dzyaloshinskii I.E., *Sov. Phys. JETP*, **26** (1968) 449.
[38] Wunner G., Ruder H. and Herold H., *J. Phys. B: At. Mol. Phys.*, **14** (1981) 765; Bhatia W.B., Namrata Chopra and Panchapakesan N., *Astrophys. J.*, **388** (1992) 131.
[39] Ackermann J., Shertzer J. and Schmelcher P., *Phys. Rev. Lett.*, **78** (1997) 199.
[40] Lamb W.E., *Phys. Rev.*, **85** (1952) 259; Lewis M.L. and Huges V.W., *Phys. Rev. A*, **8** (1973) 625.
[41] Pineda A. and Soto J., *Phys. Rev. D*, **59** (1998) 016005.
[42] Rich A., *Rev. Mod. Phys.*, **53** (1981) 127 and references therein.
[43] Mills A.P *et al*, *Phys. Rev. Lett.*, **34** (1975) 1541; Chu S., Mills A.P. and Hall J.L., *Phys. Rev. Lett.*, **52** (1984) 1689; Ziock K.P. *et al*, *J. Phys. B*, **23** (1990) 329.
[44] Halpern O., *Phys. Rev.*, **94** (1954) 904;
[45] Feinberg G., Rich A. and Sucher J., *Phys. Rev. A*, **41** (1990) 3478.
[46] Curry S.M., *Phys. Rev. A*, **7** (1973) 447; Dermer C.D. and Weisheit J.C., *Phys. Rev. A*, **40** (1989) 5526.
[47] Gallagher T.F., *Rydberg Atoms* (Cambridge University Press) 2005.
[48] Shore B.W., *The theory of coherent atomic excitation* (John Wiley & Sons) 1990.
[49] Sobelman I.I., *Atomic Spectra and Radiative Transitions* (Springer Verlag) 1979.